ACS Catalysis

Research Article

pubs.acs.org/acscatalysis

Mechanistic Insight into the Au-3d Metal Alloy-Catalyzed Borohydride Electro-Oxidation: From Electronic Properties to Thermodynamics

Ryan Lacdao Arevalo,[†,∥] Mary Clare Sison Escaño,[§] and Hideaki Kasai*[,†,‡]

[†]Department of Precision Science & Technology and Applied Physics and [‡]Center for Atomic and Molecular Technologies, Osaka University, 2-1 Yamadaoka, Suita, Osaka 565-0871, Japan

[§]Graduate School of Engineering, University of Fukui, 3-9-1 Bunkyo, Fukui 910-8507, Japan

ABSTRACT: Recent theoretical and experimental findings have motivated the use of 3d transition metals as alloying elements to improve the performance of Au for the electro-oxidation of borohydride. In this paper, we provide mechanistic insights into the electrochemical oxidation of borohydride on pure Au and Au-3d alloys (Au_3M with M = Cr, Mn, Fe, Co, Ni) using first principles calculations. We found that the initial oxidative adsorption of borohydride is the least exothermic among the elementary reactions considered for the complete eight-electron oxidation process. Interestingly, Au-3d metal alloy surfaces promote this oxidation step at a lower electrode potential compared to pure Au due the enhanced stability of borohydride on these alloy surfaces. The most negative borohydride oxidation potential is achieved by M = Co, followed by Fe, Ni, Mn, and Cr in order of increasing electrode potential. Subsequent to the initial oxidative adsorption of borohydride, the dehydrogenations of BH_3*, BH_2OH*, and $BH(OH)_2$* are endothermic on pure Au at very low potentials. However, these activated and possibly limiting elementary reaction steps are more exothermic on Au-3d alloys than on pure Au. Following the adsorption of borohydride on the surface, all elementary reaction steps for the complete electro-oxidation process proceed downhill in energy at a lower electrode potential on Au-3d alloys than on pure Au.

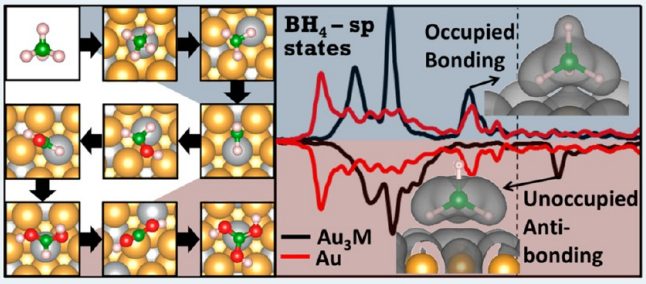

KEYWORDS: *borohydride oxidation, Au alloys, 3d transition metals, electrochemical modeling, density functional theory*

1. INTRODUCTION

The burgeoning demand for energy over the past years necessitates the research and development of alternative and reliable energy sources for the future. Hydrogen fuel cells offer an enormous potential as an alternative source of energy over combustion systems because of efficient power generation and zero greenhouse gas emission.[1−4] The issues of hydrogen storage and gas handling safety concerns, however, limit the use of hydrogen fuel cells especially for small-scale power applications.[5] Improvements were attained through the "direct feeding" of liquid hydrogen-rich fuels to the anode of the fuel cell. Among the direct-liquid-fed fuel cells, the direct borohydride fuel cell (DBFC) has recently gained considerable research attention due to its promising potential to generate high power density for portable power applications. DBFC is an alkaline-based fuel cell that operates using a base-stabilized aqueous borohydride solution as the anode fuel and oxygen at the cathode (Figure 1). Over an electrocatalyst selective to direct oxidation, each borohydride molecule is capable of donating a maximum of eight electrons to the electrode.

The efficiency and power density of DBFCs are limited in part by the lack of an effective anode electrocatalyst.[6−14] Among the pure metals which were experimentally studied, Au

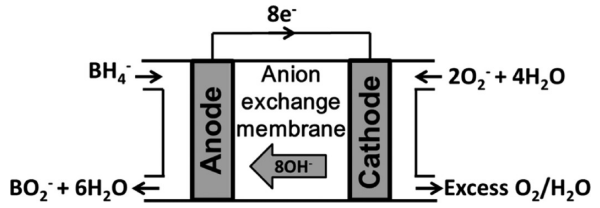

Figure 1. Schematic diagram of the direct borohydride fuel cell.

is uniquely capable of producing high Coulombic efficiency for borohydride direct oxidation, but high overpotential is necessary to achieve an appreciable rate of oxidation.[8,15,16] To address this problem, theoretical studies have proposed alloying Au with 3d (first row) transition metals which have promising properties and an interesting magnetic effect on the stability of borohydride on the surface.[17−19] Interestingly, recent experiments have shown that such Au-3d metal alloys have higher catalytic activity and require lower overpotential for borohydride oxidation than on pure Au.[20−22] However, prior to this

Received: August 26, 2013
Revised: November 6, 2013
Published: November 20, 2013

   dx.doi.org/10.1021/cs400735h | *ACS Catal.* 2013, 3, 3031−3040

work, the effect of alloying Au with 3d transition metals on the *elementary* reaction *steps* that comprise the overall oxidation of borohydride on the surface has not been clearly understood. In this paper, we provide theoretical insights into the electrochemical oxidation of borohydride on pure Au and Au-3d alloys using first principles calculations based on density functional theory and show that the previously determined limiting elementary steps on pure Au are very exothermic on Au-3d metal alloys. We present mechanistic insights from the fundamental electronic properties of borohydride interaction with pure and alloyed Au surfaces to the thermodynamics of elementary reactions for the overall oxidation of borohydride and show a detailed comparison of the electrochemical reaction pathways of borohydride electro-oxidation on Au and Au-3d alloys.

2. COMPUTATIONAL MODEL

The stable configuration of the adsorbed molecules considered in this study was determined by exhausting a number of possible orientations on the surface of a four-layer slab with one molecule of adsorbate for every four surface atoms. We found from our calculations that the adsorption energies of borohydride on four- and five-layer slabs differ only by 0.01 eV. Moreover, the d band, and thus the electronic properties of the surface, has not changed considerably as the thickness of the slab is increased. The adsorbate and the top two layers of the slab were fully relaxed in all directions while the bottom two layers were held fixed at their bulk structure. Each slab is separated by ∼12.0 Å of vacuum, which is large enough to avoid the surface atom interaction along the z axis with neighboring unit cells. The adsorption energy, E_{ads}, of each molecule studied in this work was computed by taking the difference between the total energy of the adsorbate-slab system in the lowest energy adsorption configuration and the summed energies of the optimized clean surface and the gas-phase molecule. Optimizations of isolated gas-phase molecules were performed with one free molecule within a 25 × 25 × 25 Å unit cell.

An analysis of the thermodynamics of reactions requires the calculations of free energies. The Gibbs free energy G_{A^*} of adsorbed species A^* was calculated by adding the DFT calculated total energy to the Helmholtz vibrational energy:

$$F_{vib}(\nu_i, T) = \frac{1}{2}\sum_i \left\{ h\nu_i + 2k_BT \ln\left[1 - \exp\left(-\frac{h\nu_i}{k_BT}\right)\right]\right\} \quad (1)$$

Here, the surface bound molecules are denoted by an asterisk (*) while h, k_B, ν_i, and T in eq 1 are Planck's constant, the Boltzmann constant, harmonic vibrational frequency, and temperature, respectively. The Gibbs free energies ($G_{A^-_{aq}}$) of aqueous phase species ($BH^-_{4,aq}$, OH^-_{aq} and H_2O_{aq}) for an arbitrary concentration were calculated by adding the correction term for concentration variance to the Gibbs free energies (G°) of the molecules in a standard 1 M solution taken from the literature:[23]

$$G_{A^-_{aq}} = G^\circ + k_BT \ln[A^-] \quad (2)$$

G° consists of the free energy of gas phase molecule/ion and solvation free energy of the molecule/ion at the atmospheric pressure and ambient temperature.[23]

The calculated lattice constant for fcc Au is 4.18 Å, in excellent agreement with other DFT study.[24] Au is known to form stable alloys such as Au_3M (M = Cr, Mn, Fe, Co, Ni) with the $L1_2$ structure which have been successfully synthesized in the laboratory and examined using a variety of experimental techniques, such as XRD and TEM.[25−29] We used this structure to model the alloys of Au and 3d metals. We note that DBFC works in an alkaline media which is noncorrosive for nonprecious electrodes such as the first row transition metals. There are experiments in the literature[20−22] on the oxidation of borohydride in aqueous alkaline media that utilized Au-3d alloys with varied initial compositions of surface Au and 3d metal atoms. For Au−Ni alloy in particular, it was found that surface Au and Ni atoms are oxidized at potentials of around 0.5 V vs NHE. This is much higher than the oxidation potential for borohydride oxidation on Au-3d alloys reported in this manuscript (between −0.60 and −0.32 V vs NHE) and in the experiments described. Thus, the oxidation of nickel to nickel hydroxide in an alkaline media proceeds not within the range of borohydride oxidation potential. As such, the electroactive surface areas of such a catalyst have both Au and Ni atoms. Moreover, it was found that the DBFC anode that utilizes a carbon supported Au−Ni alloy with a surface electroactive Au/Ni composition of 4.1:1 (determined by surface voltammetry in 3.0 M NaOH) gave the best performance for borohydride oxidation. The (111) facet of the Au_3M metal alloys was used to rule out the structural differences between different surfaces and to extract meaningful trends in the properties as a function of the substrate identity. The calculated lattice constants are reported in Table 1, which are in excellent agreement with experiments.[25]

Table 1. Lattice Constants, Bond Lengths, and BH_4 Adsorption Energies on Au (111) and Au_3M(111) (M = Cr, Mn, Fe, Co, Ni)

(111) surface	lattice constant (Å)	B−M bond length (Å)	B−H bond length (Å)
Au_3Cr	4.07	2.07	1.28
Au_3Mn	4.05	2.11	1.26
Au_3Fe	4.04	2.01	1.28
Au_3Co	4.03	1.84	1.36
Au_3Ni	4.03	1.93	1.32
Au	4.18		1.26

Spin-polarized DFT calculations were carried out using the Vienna ab initio simulation package (VASP).[30−33] Harmonic vibrational frequencies were calculated using the finite difference method with step size of 0.02 Å. The interaction between ions and electrons was described using the projector augmented wave (PAW) method.[34,35] Plane wave basis sets were employed with an energy cutoff of 400 eV. The exchange-correlation term was described using generalized gradient approximation (GGA) based on the Perdew−Burke−Ernzerhof (PBE) functional.[36,37] The electric dipole correction layer in the vacuum area was used to cut the dipole interactions between the repeated image layer systems. The surface Brillouin zone integrations were performed on a grid of 4 × 4 × 1 Monkhorst-Pack k-points[38] using Methfessel−Paxton smearing[39] of σ = 0.2 eV. A conjugate-gradient algorithm[40] was used to relax the ions into their ground state. The convergence of numerical results with respect to the slab thickness, the kinetic energy cutoff, and the k-point was established.

dx.doi.org/10.1021/cs400735h | ACS Catal. 2013, 3, 3031−3040

3. RESULTS AND DISCUSSION

3.1. Borohydride Adsorption Structure. The stable adsorption configuration of borohydride on Au(111) is shown in Figure 2a. Borohydride adsorbs on the surface with

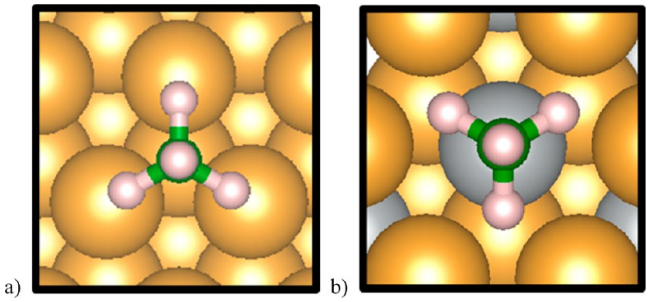

Figure 2. The optimal adsorption configuration of borohydride on (a) Au(111) and (b) $Au_3M(111)$ surfaces.

B at the hollow site and three H atoms at the top sites. The B−H bond length is 1.26 Å, which is in very close agreement with other DFT studies.[23,24] An analysis of the density of states (DOS) projected on surface Au atoms for clean and adsorbed systems shows that the shifting and broadening of Au states upon borohydride adsorption are prominent only for the spatially compatible orbitals with the BH_4-sp states. In particular, BH_4-sp states interact mainly with the s and d_{zz} (or d_{z^2}) states of surface Au atoms. The hybridization of these states can be seen in Figure 3, most noticeably in an energy

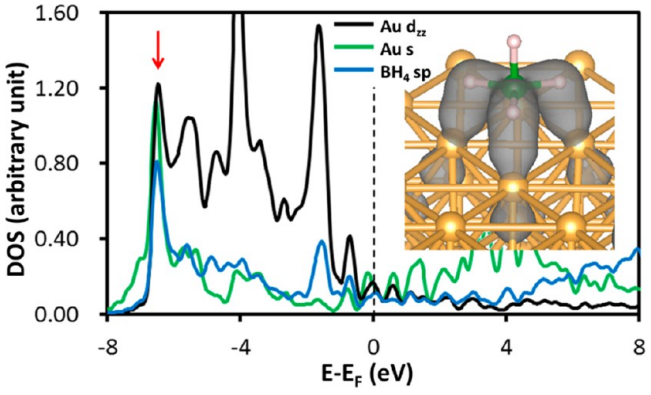

Figure 3. The density of states projected on the d_{zz} (black) and s (green) states of surface Au atoms and BH_4-sp states (blue). The inset figure shows the partial charge density plot projected at an identified bonding state denoted by the red arrow.

range of around −7.0 to −6.0 eV. Thus, the molecular structure of borohydride on Au can be characterized by the BH_4-sp hybridization with the s−d_{zz} states of Au. We show in the inset of Figure 3 a partial charge density distribution projected using a 0.01 electron/a_o^3 isosurface value at an identified bonding state (denoted by red arrow). Here, the mixing between the charge density of BH_4 and the metal is very evident.

For the Au alloys, borohydride tends to "seek" the alloying metal by adsorbing on the surface with B on top of the alloying metal M and H atoms on the hollow sites as shown in Figure 2b. B bonds directly with the alloying metal M unlike in the case of pure Au, wherein the H atoms bond directly with Au atoms. As shown in Table 1, the B−H bond lengths of borohydride on all of these alloys fall within the previously set B−H bond lengths (1.26−1.49 Å) for the case of molecularly adsorbed borohydride.[18,24] For $Au_3M(111)$ with M = Cr, Mn, and Fe, the B−H bond lengths are almost the same as that for pure Au (1.26−1.28 Å). While for M = Co and Ni, the B−H bond lengths are more elongated (1.36 and 1.32 Å respectively). To understand this, we analyzed the DOS projected on the surface alloying atom M for the clean and adsorbed systems. For all of these alloys, the components of the d band that protrude out of the surface (d_{zz}, d_{xz}, d_{yz}) interact with borohydride. However, the shift and formation of new peaks for "surface-parallel" components of the d band (d_{xy} and $d_{x^2-y^2}$) are noted only for M = Co and Ni alloys. We show this in Figure 4 using the Local-DOS of Fe (representing Au_3M

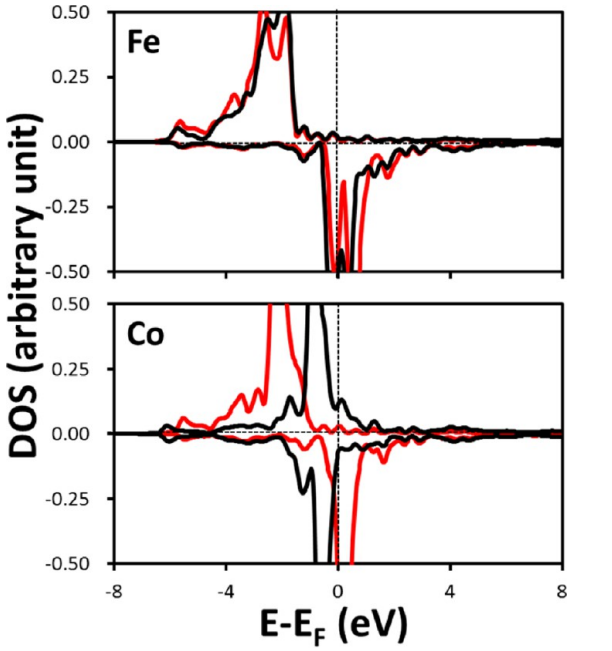

Figure 4. Density of states projected on d_{xy,x^2-y^2} components of the d band of Fe (to represent the M = Cr, Mn, and Fe cases) and Co (to represent the M = Co and Ni case). The red and black curves correspond to the clean surface and the surface with adsorbed borohydride, respectively. The positive and negative values of the density of states correspond to spin-up and spin-down states, respectively.

alloys with M = Cr, Mn and Fe) and Co (representing Au_3M alloys with M = Co and Ni) atoms projected on d_{xy} and $d_{x^2-y^2}$ states. This happens because borohydride adsorbs at a closer distance to the surfaces of Au_3Co and Au_3Ni (B−M bond length in Table 1) compared to other alloys studied. Thus, the interaction of borohydride with surface-parallel components of the d band leads to further elongation of the borohydride B−H bonds for M = Co and Ni cases. It can be argued from Figure 4 that the magnetic moment of Co has almost diminished upon borohydride adsorption (from 1.905 μ_B to 0.293 μ_B). However, this large decrease in the magnetic moment of Co is not observed for Ni (from 0.328 μ_B to 0.111 μ_B). Thus, the demagnetization of the substrate can be ruled out as the cause of the shifting of DOS peaks for d_{xy} and $d_{x^2-y^2}$ components of the d band of Co and Ni. The elongated B−H bonds for M = Co and Ni cases make the structure of borohydride vulnerable to changes triggered by external perturbations. Interestingly, He and co-workers found that Au−M (M = Co and Ni) catalysts

dx.doi.org/10.1021/cs400735h | ACS Catal. 2013, 3, 3031−3040

can cause partial hydrolysis of BH_4^- while no activity for hydrolysis was found for M = Fe.[20]

3.2. Borohydride Oxidative Adsorption. The oxidative adsorption of the borohydride anion on pure Au is first discussed in this subsection to make relevant comparisons with Au alloys. Such an electrochemical reaction is taken to require a substitution of an initially adsorbed water molecule on the surface:

$$BH_{4,aq}^- + H_2O^* \rightarrow BH_4^* + H_2O_{aq} + e^- \quad (3)$$

From this, the potential-dependent free energy of adsorption $\Delta G_{ads}(\varphi)$ can be calculated by taking the difference between the free energies of the products and reactants:

$$\Delta G_{ads}(\varphi) = G_{BH_4^*} + G_{H_2O_{aq}} - G_{H_2O^*} - G_{BH_{4,aq}^-} - e\varphi \quad (4)$$

where φ is the electrode potential relative to an absolute vacuum reference. The normal hydrogen electrode (NHE) potential has values between 4.4 and 4.8 V referenced to an absolute vacuum.[41] In this study, a value of 4.6 V is selected. Thus,

$$\varphi = \varphi_{NHE} + 4.6V \quad (5)$$

where φ_{NHE} is the electrode potential referenced to NHE. This model approximates the energy of the transferred electron to be linearly dependent on the electrode potential.[23,42−45] This approach, developed by the group of Norskov,[45] is computationally efficient in considering a large number of elementary reactions that involve many adsorbed species but neglects the interactions between the adsorbates and the solvent. Rostamikia and Janik[43] have shown that this model produces identical $\Delta G_{ads}(\varphi)$ for borohydride oxidative adsorption on Au(111) with the double-reference method of Neurock et al.,[46,47] which includes the interaction of surface bound species with solvent molecules near the surface as well as the potential dependence of adsorbate−metal interactions in an electrochemical double layer model.

In order to elucidate the effect of borohydride surface adsorption coverage and aqueous BH_4^- molar concentration in our simulation, we present the oxidation potential φ_{ox} as a function of BH_4^- molar concentration for different adsorbate coverage in Figure 5. φ_{ox} is defined to be the electrode potential vs NHE, wherein borohydride oxidative adsorption starts to become favorable ($\Delta G_{ads} = 0$). As shown in Figure 5, for a particular surface adsorption coverage, increasing the molar concentration of BH_4^- results in a more negative oxidation potential. At the range of 0 to 0.1 M, the oxidation potential decreases rapidly for both 1/4 and 1/9 ML coverages with increasing borohydride molar concentration. On the other hand, for a particular BH_4^- molar concentration, decreasing the adsorbate coverage from 1/4 to 1/9 ML shifts the oxidation potential to a more negative value by 0.05 V. Alternatively, borohydride oxidative adsorption is favorable at an electrode potential 0.05 V lower for 1/9 ML than for 1/4 ML surface coverage.

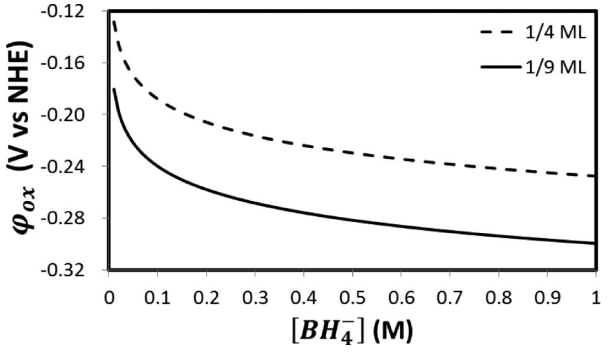

Figure 5. The borohydride oxidation potential as a function of aqueous borohydride solution molar concentration for different adsorbate coverage.

In Figure 6, we show the ΔG_{ads} vs φ_{NHE} plots for pure Au (red plots) for $[BH_4^-]$ = 0.03 M and $[OH^-]$ = 2.0 M concentrations for different adsorbate coverages. These molar concentrations are typically used in borohydride electro-oxidation kinetic studies.[8] The oxidative adsorption of borohydride on the Au(111) surface is favorable ($\Delta G_{ads} < 0$) at −0.20 and −0.15 V vs NHE for adsorbate coverages of 1/9 and 1/4 ML, respectively. This is consistent with experimental results which show that very little current can be drawn from the electro-oxidation of borohydride on Au(111) within the energy range of the experimental open-circuit potential (−0.8 V) to −0.3 V vs NHE.[15] Also, cyclic voltammetry results for 0.03 M $NaBH_4$ in 2 M NaOH on a Au disk electrode have shown an oxidation peak at approximately −0.2 V vs NHE at a scan rate of 0.025 V/s, which is attributed to the direct oxidation of borohydride.[8,48] The relatively high potential requirement for the adsorption of borohydride on Au is due to the reported weak interaction of borohydride on the Au surface.[19,24]

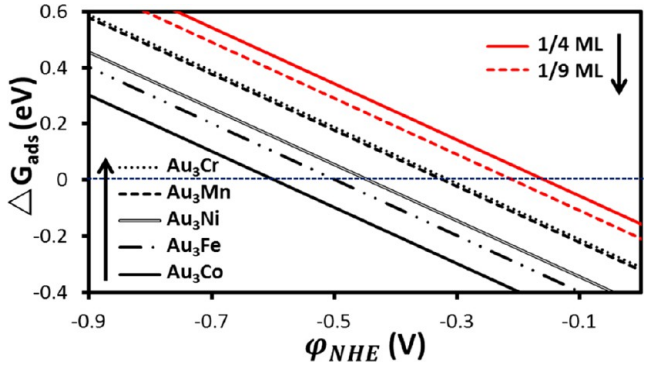

Figure 6. The free energy of adsorption of borohydride as a function of electrode potential vs NHE for different surfaces. Red plots are for the case of Au(111) at different adsorbate coverage, while the black plots are for the Au alloys at an adsorbate coverage of 1/4 ML.

For the Au-3d alloys (black plots in Figure 6), the oxidative adsorption of borohydride is favorable at a potential range of −0.60 to −0.32 V vs NHE which is 0.17 to 0.45 V lower in potential compared to pure Au. The most negative potential is achieved by M = Co, followed by Fe, Ni, Mn, and Cr in order of increasing electrode potential. Lower oxidation peak potential was experimentally observed on Au-3d metal alloy catalysts compared to pure Au.[20−22] The presence of a 3d metal on the surface promotes greater stability for adsorbed borohydride, making the adsorption favorable at a lower potential compared to pure Au. We explain this by analyzing the DOS projected on the surface metal atoms for pure Au and a clean Au_3Co slab as a representative alloy. Au_3Co is chosen since it gives the most negative potential for borohydride oxidation. As shown in Figure 7a, the d band of the clean

dx.doi.org/10.1021/cs400735h | ACS Catal. 2013, 3, 3031−3040

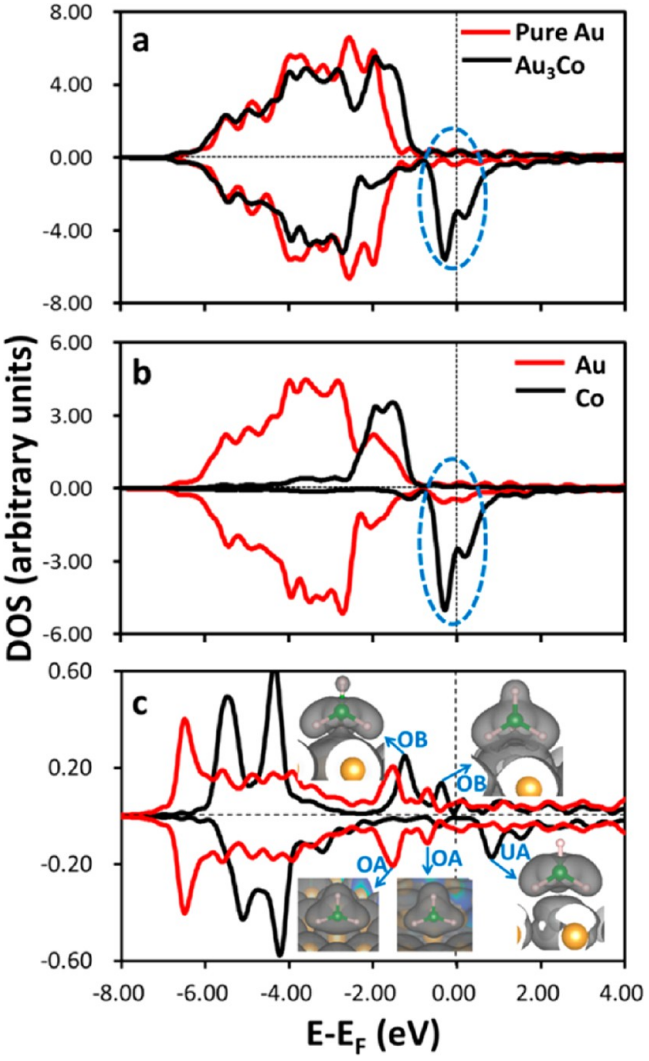

Figure 7. (a) The d band projected on pure Au (red) and clean Au_3Co (black) surfaces, (b) atom projected d band of a clean Au_3Co surface, and (c) sp states of borohydride adsorbed on pure Au (red) and Au_3Co (black). States near the Fermi level are shown by the blue dashed ellipses in a and b. Inset figures in c denoted as OB, OA, and UA correspond to occupied bonding, occupied antibonding, and unoccupied antibonding states, respectively. The positive and negative values of density of states correspond to spin-up and spin-down states, respectively.

surface of pure Au is fully occupied. When this Au−d band hybridizes with the sp state of borohydride, both the derived sp−d bonding and antibonding states are occupied as shown in Figure 7c (red curve). The occupied states near the Fermi level (insets labeled OA) have antibonding characteristics which contribute to a repulsive interaction. On the other hand, for the clean Au_3Co surface (black curve in Figure 7a), spin-down states around the Fermi level have appeared as indicated by the dashed ellipse. These states are mainly Co states, as shown in Figure 7b. The lower band in Figure 7a for Au_3Co is mainly from Au. Consequently, when the high-lying d band of Au_3Co hybridizes with the borohydride sp states, the derived antibonding state of the sp−d interaction (inset labeled UA in Figure 7c) is upshifted and unoccupied unlike on pure Au. The corresponding bonding states (insets labeled OB in Figure 7c) below the Fermi level are occupied and are due to B−Co (at energy of around −1.30 eV) and H−Co (at energy of −0.45 eV) bonding interactions. For the d band projected on the surface of other clean Au_3M slabs, there is also an emergence of states near the Fermi level in the same energy range as that for Au_3Co. The same bonding mechanism as for the case of Au_3Co explains the enhanced stability of borohydride on other Au_3M surfaces compared to pure Au.

3.3. Adsorption of Possible Intermediate Species.

Aqueous borohydride anion oxidizes to borate anion via the suggested eight-electron process:

$$BH^-_{4,aq} + 8OH^-_{aq} \rightarrow B(OH)^-_{4,aq} + 4H_2O_{aq} + 8e^- \quad (6)$$

Rostamikia and Janik proposed a BO_xH_y ($x, y = 0, 1, 2, 3$) type of molecules for possible elementary intermediate species for the eight-electron borohydride electro-oxidation.[23,43] We show in Figure 8a our calculated optimal adsorption configuration of these molecules on a Au(111) surface at a coverage of 1/4 ML. This confirms the earlier reported results of Rostamikia and Janik for 1/9 ML adsorbate coverage.[23] A comparison of adsorption energies of these species is shown by red plots in Figure 9. Regions of weak binding, intermediate adsorption energy, and strong binding of molecules are color-coded.

The adsorbed species on Au(111) which are weakly bound (E_{ads} < 1.00 eV) on the surface are BH_3*, BH_2OH*, BH_2O*, BHO*, BOOH*, and $B(OH)_3$*. The adsorption configuration of BH_3* is similar to BH_4* such that the H atoms reside on the top sites while B is at the hollow site. BH_2OH* binds on the surface via a Au−H bond. BH_2O* adsorbs with O on top of the surface Au atom and B at the bridge site. BHO* has a linear structure with B at the top site and B−H and B−O bonds pointing toward bridge sites. For BOOH*, O resides near the top of the surface Au atom, while B is at the bridge site. $B(OH)_3$* adsorbs on the surface with its molecular plane parallel to the surface and B at the hollow site.

The species with intermediate adsorption energies (1.00 eV < E_{ads} < 3.00 eV) are BH_2*, BHOH*, BOH*, $BH(OH)_2$*, BO*, BHOOH*, $B(OH)_2$*, BHO_2*, and BH_3OH*. BH_2* forms a bent structure with an inner angle of 104°. BHOH* adsorbs with B at the bridge site and B−H and O−H bonds pointing away and toward the surface, respectively. BOH* adsorbs on the surface with B at the hollow site and O−H bond tilted toward the top site at 27° with respect to the surface. For $BH(OH)_2$*, B is closer to the surface than the case of O atoms. BO* adsorbs with B at the hollow site and the B−O bond perpendicular to the surface. BHOOH* adsorbs with O and H atoms at the top sites. For $B(OH)_2$*, its molecular plane is parallel to the hollow-top-hollow site plane with the hydroxyl group pointing toward the surface and B at the top site. For BHO_2*, one O atom is directly bound on top of Au, while the B−H bond is perpendicular to the surface. BH_3OH* binds similarly with BH_3* and BH_4* with H at the top sites and B at the hollow site.

The strongly adsorbed molecules with E_{ads} > 3.00 eV are BH* and B*. BH* has the strongest binding energy among the species considered and is adsorbed with B at the hollow site and B−H bond perpendicular to the surface. Because of the very strong adsorption of these species on the surface, these molecules can potentially poison the surface. However, conversion of these molecules to other surface bound species through B−H bond dissociation or B−O bond formation proceeds downhill in energy, as will be shown in later discussions.

For the Au-3d alloys, Figure 8 shows that the presence of the alloying metal M on the surface changes the optimal adsorption

dx.doi.org/10.1021/cs400735h | ACS Catal. 2013, 3, 3031−3040

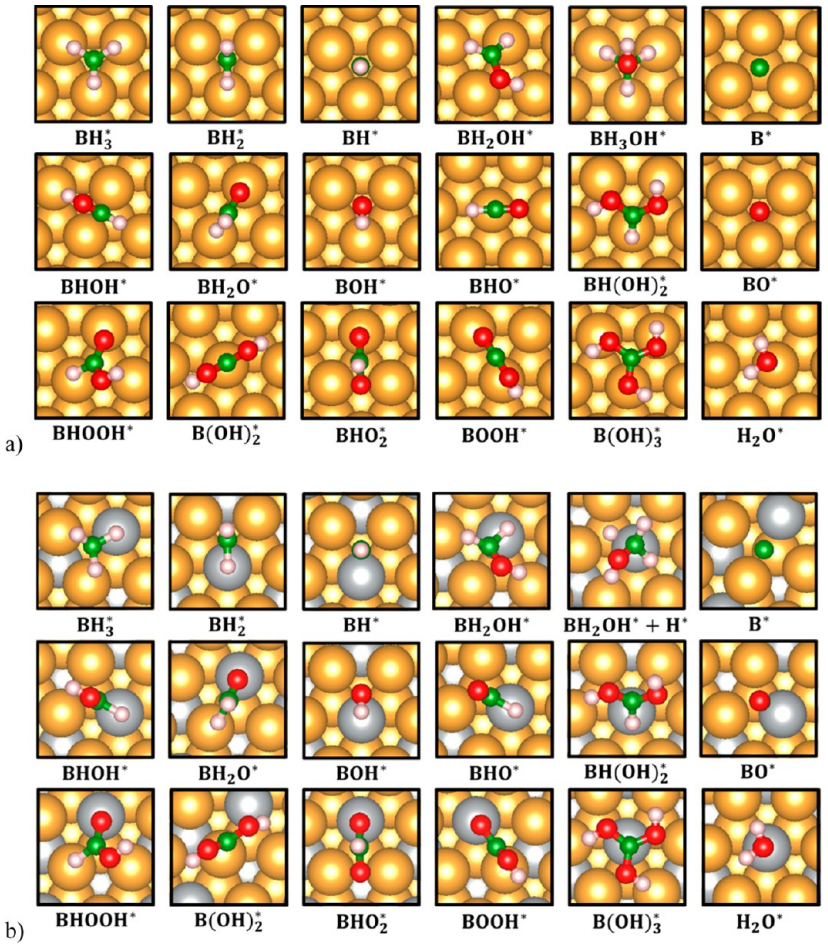

Figure 8. The optimal adsorption configurations of different molecules on pure Au (a) and Au_3M alloys (b). Yellow, gray, green, red, and pink spheres correspond to Au, Ni, B, O, and H atoms, respectively.

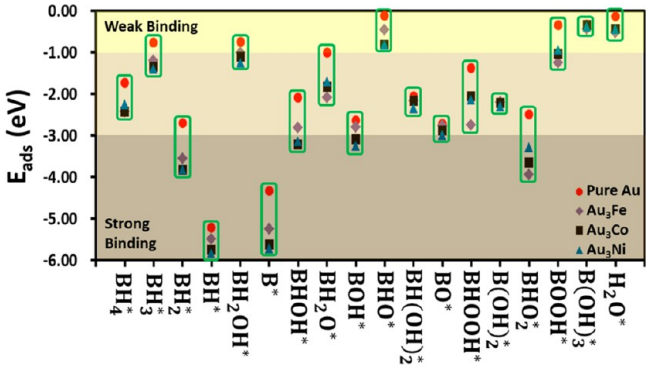

Figure 9. The adsorption energy E_{ads} of different species considered in this study for different surfaces. The plot is color-coded to show the region of weak binding, intermediate binding energies, and strong binding of molecules.

configurations of the molecules. Figure 8b can represent the adsorption configurations of adsorbed molecules for all the Au-3d alloy surfaces considered since the difference in the bond lengths and angles of adsorbed species on the different alloy surfaces are small. The most notable difference in the adsorption configurations of the molecules on Au and Au-3d alloys is seen for BHO* and $B(OH)_3$*. BHO* has a linear structure on pure Au but a bent structure on the Au alloys with the B−O bond pointing away from the surface. For $B(OH)_3$*, B resides at the M top site for the alloy surface, whereas B resides on the hollow site for pure Au. Slight difference in adsorption configurations can also be seen for other molecules.

BH_3OH^- has been speculated as an intermediate solution phase product on both pure and alloyed Au.[21,49,50] We found that molecularly adsorbed BH_3OH* is stable only on Au but not on Au-3d alloys. Optimization of BH_3OH on the Au-3d-alloy surfaces results in BH_2OH* + H*, as shown in Figure 8b. Thus, although BH_3OH* may form through surface reactions, further dehydrogenation at the surface would be very rapid. On the other hand, since BH_3* is weakly adsorbed on the surface, it can desorb to the aqueous media and hydroxylate in the solution to form BH_3OH^-.

As shown in Figure 9, all considered molecules are more stably adsorbed on the Au-3d alloys than on pure Au. The adsorption energies of $B(OH)_2$* and $B(OH)_3$* have not changed considerably. For both the pure and alloyed Au surfaces, the species which have relatively weak adsorption are BH_3*, BH_2OH*, BHO*, BOOH*, and $B(OH)_3$*, while BH* and B* have very strong adsorption energies on all surfaces.

3.4. Overall Surface Oxidation Reaction. Using aqueous borohydride anion ($BH_{4,aq}^-$) as a reference, the electrochemical reaction along the oxidation reaction coordinate is defined as

dx.doi.org/10.1021/cs400735h | ACS Catal. 2013, 3, 3031−3040

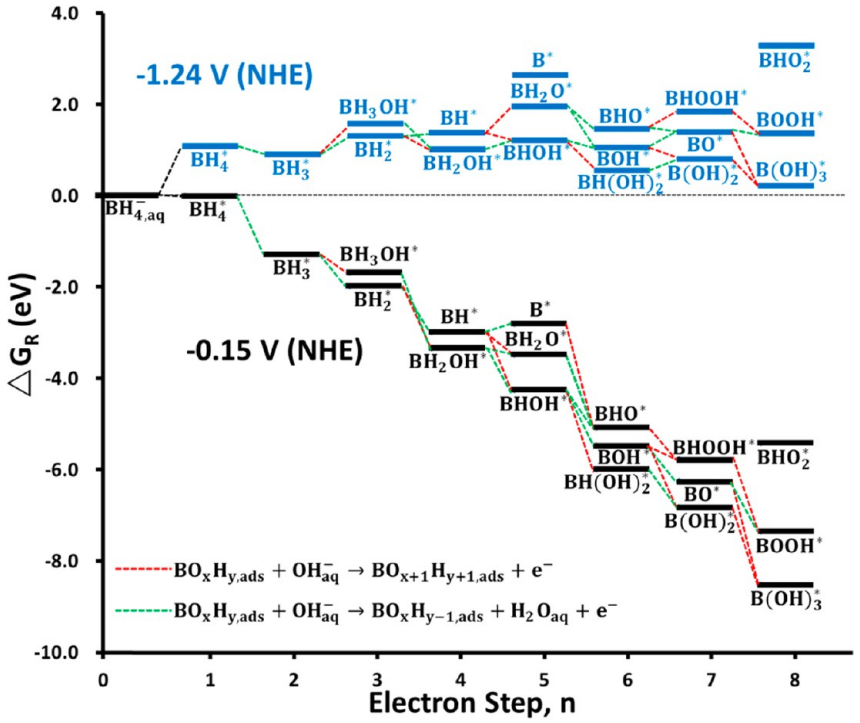

Figure 10. The potential dependent reaction free energy diagram evaluated at the theoretical equilibrium potential (−1.24 V) and at −0.15 V vs NHE for borohydride oxidation on Au(111). Reaction paths that correspond to dissociation (of B−H or O−H bond) and bond formation (of B−H, O−H, or B−O bond) are indicated by green and red dashed lines, respectively. Each step to the right corresponds to one electron step.

$$BH^-_{4,aq} + 7OH^-_{aq} + H_2O^* \rightarrow BO_xH^*_y + (3 - 2x + y)OH^-_{aq} + (5 + x - y)H_2O_{aq} + (5 + 2x - y)e^- \quad (7)$$

The free energy change for this reaction, ΔG_R, gives the relative free energy of adsorbed species $BO_xH^*_y$, which corresponds to an electron step $n = 5 + 2x - y$ as a function of electrode potential:

$$\Delta G_R = G_{BO_xH^*_y} + (3 - 2x + y)G_{OH^-_{aq}} + (5 + x - y)G_{H_2O_{aq}} - G_{BH^-_{4,aq}} - 7G_{OH^-_{aq}} - G_{H_2O^*} - (5 + 2x - y)e\varphi \quad (8)$$

This was used to construct a free energy diagram that facilitates the comparison of possible reaction paths.

For the case of pure Au, the reaction free energy diagram evaluated at the theoretical equilibrium potential (−1.24 V) and −0.15 V vs NHE with parameters T = 300 K, $[BH^-_4]$ = 0.03 M, $[OH^-]$ = 2.0 M, and 1/4 ML surface coverage is presented in Figure 10. It was shown earlier that the initial oxidative adsorption of borohydride at 1/4 ML coverage is favorable at −0.15 V vs NHE for the case of pure Au. Reaction paths that correspond to dissociation (of B−H or O−H bond) and bond formation (of B−H, O−H, or B−O bond) are indicated by green and red dashed lines, respectively. Each step to the right corresponds to one electron step. As shown in Figure 10, all elementary steps proceed downhill in energy at a potential of −0.15 V vs NHE. The formation of BH_3* is highly favorable in the second electron step at all relevant potentials. The formation of BH_2* and BH_3OH* from BH_3* is uphill in energy at the equilibrium potential and favorable only at potentials of −0.85 and −0.55 V, respectively. Further dehydrogenation of BH_3OH* to BH_2OH* is very exothermic and favorable at all potentials of interest. This agrees with experimental results that the oxidation of BH_3OH^- on Au, which is generated from NH_3BH_3 decomposition, proceeds at an approximately 0.4 V lower potential than BH^-_4.[50,51] The conversion of BH_2* to BH* through B−H bond dissociation and to BH_2OH* through B−O bond formation is favorable at all relevant potentials. At the equilibrium potential, the conversion of BH_2OH* to other species is uphill in energy and becomes favorable only at −1.05 and −0.25 V for its conversion to BHOH* and BH_2O*, respectively. The strongly adsorbed BH* can be converted to BHOH* at all potentials of interest. The conversion of BH_2O* and BHOH* to BOH* and $BH(OH)_2$* is favorable at all relevant potentials. The dehydrogenation of $BH(OH)_2$* to $B(OH)_2$* is uphill in energy at the equilibrium potential and favorable only at −0.95 V. In the final electron step, $B(OH)_3$* is highly favorable as the final adsorbed species. At −0.15 V vs NHE, BOOH* is also favored as a final adsorbed species 1.16 eV higher in energy compared to $B(OH)_3$*. Since both of these species are weakly bound on the surface, these can easily desorb to the aqueous media and hydroxylate in the solution to form $BO^-_2 \cdot nH_2O$ with n = 1 and 2 for BOOH* and $B(OH)_3$*, respectively. $B(OH)_3$*, as the final adsorbed species rather than BO_2*, was theoretically confirmed by Rostamikia and Janik.[43,52] BHO_2* is strongly adsorbed on the surface, but its formation as the final adsorbed species is unlikely due to its relatively high energy with respect to BOOH* and $B(OH)_3$*. In this reaction diagram, it can noted that subsequent to the initial oxidative adsorption of borohydride, the conversion of BH_3*, BH_2OH*, and $BH(OH)_2$* to other species through B−H bond dissociation proceeds uphill in energy at very low potentials. This is consistent with a reported DFT result that the dehydrogenation

dx.doi.org/10.1021/cs400735h | ACS Catal. 2013, 3, 3031−3040

of these species is activated and can possibly limit the overall oxidation reaction.[52]

To facilitate the comparison of reaction paths for pure and alloyed Au, we show in Table 2 the calculated ΔG_R of adsorbed species for the case of pure Au and Au_3M with M = Fe, Co, and Ni surfaces, evaluated at −0.60 V vs NHE. As discussed earlier, borohydride oxidative adsorption is favorable at this potential for the case of M = Co. For each electron step *n*, the lowest ΔG_R is set in boldface to highlight the adsorbed species with the lowest energy. For M = Co and Ni cases, the species that yield the lowest energy for each electron step is the same as that of pure Au. On the other hand, the M = Fe case differs in the seventh electron step, giving BHOOH* as the most preferred species rather than $B(OH)_2$*. Thus, the minimum energy path for the complete oxidation of borohydride on the Au alloys proceeds via the same reaction coordinate as on pure Au, except for the seventh electron step of the M = Fe case. Figure 11 shows the relative energies of the adsorbed species in the minimum energy path for borohydride oxidation on pure Au and Au alloys evaluated at −0.60 V vs NHE. At this potential, all elementary reaction steps are downhill in energy for the M = Co case (black path in Figure 11). The first electron step is the most uphill in energy for pure Au since it requires the highest electrode potential for such a reaction to proceed. However, subsequent to the initial borohydride oxidative adsorption, all elementary reaction steps are downhill in energy for both pure and alloyed Au surfaces. To further compare the elementary reaction steps on these surfaces, we show in Figure 12 the

Table 2. Relative Free Energies of Adsorbed Species on Different Surfaces

		ΔG_R (eV)[a]			
n	adsorbed species	Au	Au_3Fe	Au_3Co	Au_3Ni
1	BH_4^*	**0.44**	**0.12**	**0.00**	**0.16**
2	BH_3^*	**−0.38**	**−0.43**	**−0.67**	**−0.71**
3	BH_2^*	**−0.63**	**−1.10**	**−1.46**	**−1.44**
4	BH*	−1.19	−1.10	−1.46	−1.53
	BH_2OH*	**−1.55**	**−1.46**	**−1.64**	**−1.76**
	BH_3O*	−1.00	−0.79	−0.62	−0.42
5	B*	−0.56	−1.12	−1.59	−1.68
	BHOH*	**−2.01**	**−2.37**	**−2.88**	**−2.80**
	BH_2O*	−1.24	−1.93	−1.76	−1.64
6	BOH*	−2.77	−2.57	−2.96	−3.12
	BHO*	−2.38	−2.37	−2.81	−2.82
	$BH(OH)_2^*$	**−3.30**	**−3.05**	**−3.16**	**−3.33**
7	BO*	−3.10	−2.79	−2.98	−3.09
	BHOOH*	−2.63	**−3.59**	−3.00	−3.10
	$B(OH)_2^*$	**−3.67**	−3.28	**−3.38**	**−3.48**
8	BHO_2^*	−1.83	−2.92	−2.72	−2.35
	BOOH*	−3.77	−4.26	−4.14	−4.05
	$B(OH)_3^*$	**−4.92**	**−4.66**	**−4.66**	**−4.70**

[a]Evaluated at −0.60 V vs NHE.

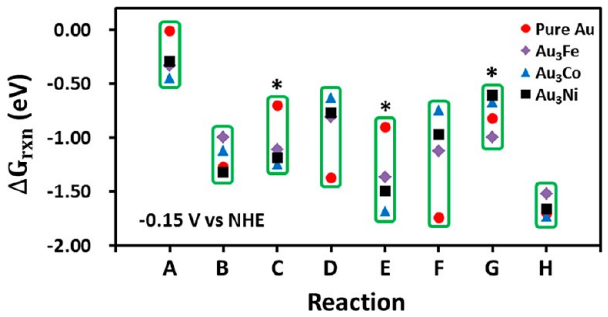

Figure 12. Reaction free energy change evaluated at −0.15 V vs NHE for reactions that correspond to the minimum energy path for the borohydride eight-electron oxidation process on different surfaces.

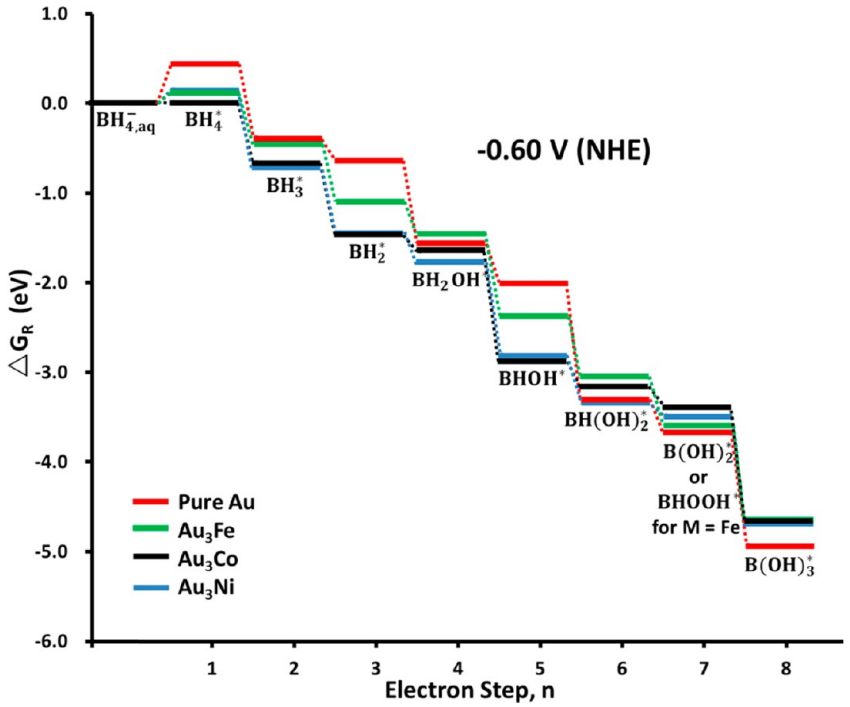

Figure 11. Relative free energy of adsorbed species along the minimum energy path for the borohydride eight-electron oxidation process on different surfaces, evaluated at −0.60 V vs NHE.

dx.doi.org/10.1021/cs400735h | ACS Catal. 2013, 3, 3031−3040

reaction free energy change ΔG_{rxn} evaluated at −0.15 V vs NHE for reactions that correspond to the minimum energy path:

$$BH_{4,aq}^{-} + H_2O^* \rightarrow BH_4^* + H_2O_{aq} + e^- \quad (A)$$

$$BH_4^* + OH_{aq}^- \rightarrow BH_3^* + H_2O_{aq} + e^- \quad (B)$$

$$BH_3^* + OH_{aq}^- \rightarrow BH_2^* + H_2O_{aq} + e^- \quad (C)$$

$$BH_2^* + OH_{aq}^- \rightarrow BH_2OH^* + e^- \quad (D)$$

$$BH_2OH^* + OH_{aq}^- \rightarrow BHOH^* + H_2O_{aq} + e^- \quad (E)$$

$$BHOH^* + OH_{aq}^- \rightarrow BH(OH)_2^* + e^- \quad (F)$$

$$BH(OH)_2^* + OH_{aq}^- \rightarrow B(OH)_2^* + H_2O_{aq} + e^- \quad (G)$$

or

$$BH(OH)_2^* + OH_{aq}^- \rightarrow BHOOH^* + H_2O_{aq} + e^- \text{ (for M = Fe case)}$$

$$B(OH)_2^* + OH_{aq}^- \rightarrow B(OH)_3^* + e^- \quad (H)$$

or

$$BHOOH^* + OH_{aq}^- \rightarrow B(OH)_3^* + e^- \text{ (for M = Fe case)}$$

This potential was chosen such that all reaction steps are exothermic for all of the surfaces considered. The reaction steps which were previously pointed out as possible limiting steps subsequent to the initial adsorption of borohydride for the case of pure Au, viz., dehydrogenation of BH_3*, BH_2OH*, and $BH(OH)_2$*, are denoted by an asterisk (reactions C, E, and G). The dehydrogenation of BH_3* and BH_3OH* is more exothermic on Au alloys than on pure Au. For $BH(OH)_2$*, its dehydrogenation on M = Fe is more exothermic than on pure Au with BHOOH* as the dehydrogenation product rather than $B(OH)_2$*. The conversion of BH_2* and BHOH* through B−O bond formation (reactions D and F) is less exothermic on Au alloys than on pure Au. However, it was previously shown that such B−O formation reactions are fast and nonactivated.[52] The formation of $B(OH)_3$* as the final adsorbed product is highly exothermic for all surfaces. Figure 12 clearly shows that the least exothermic elementary reaction is the initial oxidative adsorption of borohydride (reaction A).

From these discussions, the improved performance of borohydride oxidation on Au-3d alloys can be drawn. First, the initial oxidative adsorption of borohydride on the surface can proceed at a lower electrode potential on Au-3d alloys compared to pure Au due to the enhanced stability of borohydride on these alloy surfaces. Second, the identified activated elementary reactions (subsequent to the initial adsorption of borohydride) on pure Au are more exothermic on Au-3d alloys. Assuming that activation barriers scale with ΔG in a Brønsted−Evans−Polanyi-type relationship,[53,54] the more exothermic reactions for these activated elementary steps can result in improved kinetics of borohydride oxidation.

4. CONCLUSION

A mechanistic study for the complete electrochemical oxidation of borohydride on Au(111) and Au_3M(111) (M = Cr, Mn, Fe, Co, Ni) surfaces using first principles calculations based on density functional theory is presented. Au-3d metal alloy surfaces promote the initial oxidative adsorption of borohydride at a lower electrode potential compared to pure Au due to the enhanced stability of borohydride on these alloy surfaces, which is attributed to the emergence of states around the Fermi level in the surface d band of the alloy surfaces with respect to pure Au surface. The most negative oxidation potential is achieved by M = Co, followed by Fe, Ni, Mn, and Cr in order of increasing electrode potential. Subsequent to the initial oxidative adsorption of borohydride, the dehydrogenations of BH_3*, BH_2OH*, and $BH(OH)_2$* are endothermic on pure Au at very low potentials. However, these activated and possibly limiting elementary reaction steps are more exothermic on Au-3d alloys. Following the initial oxidative adsorption of borohydride, all elementary reaction steps for the complete oxidation of borohydride proceed downhill in energy for both pure and alloyed Au surfaces. These results pose significant insights into the design of efficient and low-cost catalysts for borohydride oxidation relevant to DBFC.

AUTHOR INFORMATION

Corresponding Author

*Tel.: +81(Japan)-6-6879-7857. E-mail: kasai@dyn.ap.eng.osaka-u.ac.jp.

Notes

The authors declare no competing financial interest.

‖On leave from Department of Physical Sciences, Philippine Normal University, Manila 1000, Philippines.

ACKNOWLEDGMENTS

This work is supported in part by MEXT Grant-in-Aid for Scientific Research on Innovative Areas Program (2203-22104008); Scientific Research programs (A) (24246013); and Grants for Excellent Graduate Schools (130820-140331) "Atomically Controlled Fabrication Technology;" JST ALCA Program "Development of Novel Metal-Air Secondary Battery Based on Fast Oxide Ion Conductor Nano Thickness Film" and Strategic Japan−Croatia Research Cooperative Program on Materials Sciences Program "Theoretical Modeling and Simulations of the Structural, Electronic, and Dynamical Properties of Surfaces and Nanostructures in Materials Science Research;" Osaka University Joining and Welding Research Institute Cooperative Research Program. Some of the numerical calculations presented here were done using the computer facilities at the following institutes: CMC (Osaka University), ISSP, KEK, NIFS, and YITP. R.L.A. acknowledges MEXT for scholarship grant. M.C.S.E. would like to thank the Special Coordination Funds for the Promotion of Science and Technology of the Ministry of Education, Culture and Sports (MEXT) through the Tenure Track Program for Innovative Research, University of Fukui for research funds. The authors acknowledge Prof. Elod Gyenge and Andrew Yu-Sheng Wang of the Department of Chemical and Biological Engineering of the University of British Columbia, Vancouver, Canada for fruitful collaborations through the years.

REFERENCES

(1) Frenette, G.; Forthoffer, D. *Int. J. Hydrogen Energy* **2009**, *34*, 3578−3588.
(2) Neef, H.-J. *Energy* **2009**, *34*, 327−333.
(3) Contestabile, M.; Offer, G. J.; Slade, R.; Jaeger, F.; Thoennes, M. *Energy Environ Sci.* **2011**, *4*, 3754−3772.
(4) Corbo, P.; Migliardini, F.; Veneri, O. *Renewable Energy* **2009**, *34*, 1955−1961.
(5) Mori, D.; Hirose, K. *Int. J. Hydrogen Energy* **2009**, *34*, 4569−4574.
(6) Wee, J.-H. *J. Power Sources* **2006**, *155*, 329−339.
(7) Ponce de Leon, C. P.; Walsh, F. C.; Pletcher, D.; Browning, D. J.; Lakeman, J. B. *J. Power Sources* **2006**, *155*, 172−181.
(8) Gyenge, E. *Electrochim. Acta* **2004**, *49*, 965−978.
(9) Gyenge, E.; Atwan, M.; Northwood, D. *J. Electrochem. Soc.* **2006**, *153*, A150−A158.
(10) Wee, J.-H. *J. Power Sources* **2006**, *161*, 1−10.
(11) Martins, J. I.; Nunes, M. C.; Koch, R.; Martins, L.; Bazzaoui, M. *Electrochim. Acta* **2007**, *52*, 6443−6449.
(12) Lam, V.; Kannangara, D.; Alfantazi, A.; Gyenge, E. *J. Phys. Chem. C* **2011**, *115*, 2727−2737.
(13) Lam, V.; Gyenge, E. *J. Electrochem. Soc.* **2008**, *155*, B1155−B1160.
(14) Li, Z. P.; Liu, B. H.; Arai, K.; Suda, S. J. *J. Alloys Compd.* **2005**, *648*, 404−652.
(15) Chatenet, M.; Micoud, F.; Roche, I.; Chainet, E. *Electrochim. Acta* **2006**, *51*, 5459−5467.
(16) Mirkin, M. V.; Yang, H.; Bard, A. J. *J. Electrochem. Soc.* **1992**, *139*, 2212−2217.
(17) Rostamikia, G.; Janik, M. J. *Energy Environ. Sci.* **2010**, *3*, 1262−1274.
(18) Arevalo, R. L.; Escano, M. C. S.; Gyenge, E.; Kasai, H. *Surf. Sci.* **2012**, *606*, 1954−1959.
(19) Arevalo, R. L.; Escano, M. C. S.; Wang, A.Y.-S.; Kasai, H. *Dalton Trans.* **2013**, *42*, 770−775.
(20) He, P.; Wang, X.; Liu, Y.; Yi, L. *Int. J. Hydrogen Energy* **2012**, *37*, 11984−11993.
(21) He, P.; Wang, X.; Liu, Y.; Yi, L.; Liu, X. *Int. J. Hydrogen Energy* **2012**, *37*, 1254−1262.
(22) He, P.; Wang, Y.; Wang, X.; Pei, F.; Wang, H.; Liu, L.; Yi, L. *J. Power Sources* **2011**, *196*, 1042−1047.
(23) Rostamikia, G.; Janik, M. J. *J. Electrochem. Soc.* **2009**, *156*, B86−B92.
(24) Escano, M. C. S.; Gyenge, E.; Arevalo, R. L.; Kasai, H. *J. Phys. Chem. C* **2011**, *115*, 19883−19889.
(25) Vasquez, Y.; Luo, Z.; Schaak, R. E. *J. Am. Chem. Soc.* **2008**, *130*, 11866−11867.
(26) Yamamoto, K. *Phys. Status Solidi* **1980**, *59*, 767−777.
(27) Dutkiewicz, J.; Thomas, G. *Metall. Trans. A* **1975**, *6A*, 1920−1928.
(28) Sato, H.; Toth, R. S.; Honjo, G. *J. Phys. Chem. Solids* **1967**, *28*, 137−160.
(29) Sato, H.; Toth, R. S. *J. Phys. Chem. Solids* **1966**, *27*, 413−422.
(30) Kresse, G.; Furthmuller, J. *Comput. Mater. Sci.* **1996**, *6*, 15−50.
(31) Kresse, G.; Furthmuller, J. *Phys. Rev. B* **1996**, *54*, 11169−11186.
(32) Kresse, G.; Hafner, J. *Phys. Rev. B* **1993**, *47*, 558−561.
(33) Kresse, G.; Hafner, J. *Phys. Rev. B* **1994**, *49*, 14251−14269.
(34) Blochl, P. E. *Phys. Rev. B* **1994**, *50*, 17953−17979.
(35) Kresse, G.; Joubert, J. *Phys. Rev. B* **1999**, *59*, 1758−1775.
(36) Perdew, J.; Burke, K.; Ernzerhof, M. *Phys. Rev. Lett.* **1996**, *77*, 3865−3868.
(37) Perdew, J.; Burke, K.; Ernzerhof, M. *Phys. Rev. Lett.* **1997**, *78*, 1396.
(38) Monkhorst, H. J.; Pack, J. D. *Phys. Rev. B* **1976**, *13*, 5188−5192.
(39) Methfessel, M.; Paxton, A. *Phys. Rev. B* **1989**, *470*, 3616−3621.
(40) Stich, I.; Car, R.; Parrinello, M.; Baroni, S. *Phys. Rev. B* **1989**, *39*, 4997−5004.
(41) Tsiplakides, D.; Vayenas, C. G. *Solid State Ionics* **2002**, *152*−*153*, 625−639.
(42) Arevalo, R. L.; Escano, M. C. S.; Kasai, H. *J. Phys. Chem. C* **2013**, *117*, 3818−3825.
(43) Rostamikia, G.; Janik, M. J. *Electrochim. Acta* **2010**, *55*, 1175−1183.
(44) Anderson, A. B.; Kang, D. B. *J. Phys. Chem. A* **1998**, *102*, 5993−5996.
(45) Norskov, J. K.; Rossmeisl, J.; Logadottir, A.; Lindqvist, L.; Kitchin, J. R.; Bligaard, T.; Jonsson, H. *J. Phys. Chem. B* **2004**, *108*, 17886−17892.
(46) Taylor, C. D.; Wasileski, S. A.; Filhol, J. S.; Neurock, M. *Phys. Rev. B* **2006**, *73*, 165402−165417.
(47) Filhol, J. S.; Neurock, M. *Angew. Chem., Int. Ed.* **2006**, *45*, 402−406.
(48) Ignaszak, A.; Kannangara, D. C. W.; Lam, V. W. S.; Gyenge, E. *J. Electrochem. Soc.* **2013**, *160*, H47−H53.
(49) Krishnan, P.; Yang, T.-H.; Advani, S. G.; Prasad, A. J. *J. Power Sources* **2008**, *182*, 106−111.
(50) Chatenet, M.; Lima, F. H. B.; Ticianelli, E. A. *J. Electrochem. Soc.* **2010**, *157*, B697−B704.
(51) Nagle, L. C.; Rohan, J. F. *J. Electrochem. Soc.* **2006**, *153*, C773−C776.
(52) Rostamikia, G.; Mendoza, A. J.; Hicker, M. A.; Janik, M. J. *J. Power Sources* **2011**, *196*, 9228−9237.
(53) Brønsted, N. *Chem. Rev.* **1928**, *5*, 231−338.
(54) Evans, M. G.; Polanyi, N. P. *Trans. Faraday Soc.* **1938**, *34*, 11−29.